

RESEARCH ARTICLE

Intrinsic Disruption of the M1 Cortical Network in a Mouse Model of Parkinson's Disease

Fadi Aeed, MSc,¹ Nathan Cermak, PhD,¹ Jackie Schiller, PhD,¹ and Yitzhak Schiller, MD, PhD^{1,2*}

¹The Rappaport Faculty of Medicine, Technion - Israel Institute of Technology, Haifa, Israel

²Department of Neurology, Rambam Medical Center, Haifa, Israel

ABSTRACT: Background: Parkinson's disease (PD) disrupts motor performance by affecting the basal ganglia system. Yet, despite the critical position of the primary motor cortex in linking basal ganglia computations with motor performance, its contribution to motor disability in PD is largely unknown. The objective of this study was to characterize the role of the primary motor cortex in PD-related motor disability.

Methods: Two-photon calcium imaging and optogenetic stimulation of primary motor cortex neurons was done during performance of a dexterous reach-to-grasp motor task in control and 6-hydroxydopamine-induced PD mice.

Results: Experimental PD disrupted performance of the reach-to-grasp motor task and especially initiation of the task, which was partially restored by optogenetic activation of the primary motor cortex. Two-photon calcium imaging during task performance revealed experimental-PD affected the primary motor cortex in a cell-type-specific manner. It suppressed activation of output layer 5 pyramidal tract neurons, with greater effects on freeze versus nonfreeze trials. In contrast, it did not attenuate

the initial movement-related activation response of layer 2/3 pyramidal neurons while diminishing the late inhibitory phase of their response. At the network level, experimental PD disrupted movement-related population dynamics of the layer 5 pyramidal tract network while almost not affecting the dynamics of the layer 2/3 neuronal population. It also disrupted short- and long-term robustness and stability of the pyramidal tract subnetwork, with reduced intertrial temporal accuracy and diminished reproducibility of motor parameter encoding and temporal recruitment of the output pyramidal tract neurons over repeated daily sessions.

Conclusions: Experimental PD disrupts both external driving and intrinsic properties of the primary motor cortex. Motor disability in experimental PD results primarily from the inability to generate robust and stable output motor sequences in the parkinsonian primary motor cortex output layer 5 pyramidal tract subnetwork. © 2021 International Parkinson and Movement Disorder Society

Key Words: Parkinson's disease; primary motor cortex; pyramidal tract neurons; network dynamics

***Correspondence to:** Associate Professor Yitzhak Schiller, Department of Neuroscience, the Rappaport Faculty of Medicine, Technion - Israel Institute of Technology, 1 Efron Street, Haifa 31096, Israel; E-mail: y_schiller@yahoo.com

Relevant conflicts of interest/financial disclosures: F.A. declares no competing interests and has no financial disclosures. N.C. declares no competing interests. He is presently employed by Neuralink, Fremont, California. J.S. declares no competing interests. Y.S. declares no competing interests.

Funding agencies: Israel Science Foundation (ISF) and the Prince Center for Neurodegenerative Diseases supported this study. N.C. partially supported by the Zuckerman STEM Leadership Fellowship.

Received: 10 October 2020; **Revised:** 14 December 2020; **Accepted:** 15 January 2021

Published online in Wiley Online Library (wileyonlinelibrary.com). DOI: 10.1002/mds.28538

Parkinson's disease (PD) is a common neurodegenerative disease associated with motor disability caused by loss of dopaminergic neurons innervating the basal ganglia (BG).^{1,2} The BG system is organized as a functional loop originating and terminating in the neocortex. Data from the cortex is conveyed to the BG input nuclei and processed along parallel pathways within the BG. Ultimately, the different pathways converge at the BG output nuclei, where the computational product is transmitted back to the neocortex via the thalamic ventral anterior nucleus.³⁻⁵ In the case of motor behavior, the primary motor cortex (M1) serves as the main target of the thalamocortical (TC) afferents carrying the processed BG information.⁶

M1, which controls skilled hand movements in primates and rodents,^{7,8} integrates data from several

brain regions including the BG to generate output motor commands in layer 5 pyramidal tract (PT) neurons.⁹ Thus, M1 is critically situated to mediate BG abnormalities, as is the case in PD, and motor disability.

M1 can be regarded as a dynamic system, generating temporally precise sequences of output motor commands carried out by layer 5 PT neurons to control dexterous movements.^{10–13} PD has been shown to impair the activity of M1 and to induce structural changes at the spinal level in M1.^{14–16} Yet the manner by which PD affects the dynamics of the M1 layer 5 PT network is largely unknown. To address these questions, we performed 2-photon calcium imaging from GCaMP6s-expressing M1 layer 5 PT and layer 2/3 neurons, combined with optogenetic perturbations of M1 in normal and head-fixed 6-hydroxydopamine (6-OHDA)-induced parkinsonian mice while performing a skilled reach-to-grasp motor task. These experiments allowed us to investigate the effect of experimental PD on M1 neurons both at the single-cell and network levels. In addition, as our experimental design allowed us to compare the same set of neurons before and after induction of experimental PD, we were also able to investigate the temporal and motor parameter encoding stability of the normal and parkinsonian M1 network.

Methods

Mice, Surgical Procedures, and Induction of Experimental Hemiparkinson's Disease

Experiments were performed on adult male (>8 weeks) wild-type C57BL/6 and *Slc17a7-IRESs-Cre* (*VGlut1-IRES2-Cre*) transgenic mice. Preparation of the cranial window over M1 and viral injections for labeling layer 2/3 and layer 5 PT neurons were performed as we previously described.^{17,18} Experimental hemiparkinsonism was induced by injecting 6-OHDA (3 mg/mL) into 2 striatal locations using a tilted glass pipette. For additional details, see supplemental data.

In Vivo 2-Photon Calcium Imaging and Optogenetics

Two-photon calcium imaging combined with synchronized behavioral tracking via high-speed cameras was performed as previously described.^{17,18} We imaged layer 2/3 and layer 5 neurons at depths of 120–250 and 500–600 μm , respectively, below pia. Optogenetic stimulation was performed in wild-type and *Sim1-kj18-Cre* mice expressing channelrhodopsin using laser pulse trains administered via the cranial window (see Fig. 2). For additional details, see supplemental data.

Training and Behavioral Tracking of the Reach-to-Grasp Motor Task

Training and behavioral tracking of the reach-to-grasp task were performed as previously described.¹⁸ Performance of the reach-to-grasp task was monitored using 3 discrete motor milestones: lift, defined as the time when the forepaw detached from the perch; grab, defined as the time when forepaw fingers started to close around the food pellet; at mouth, defined as the time the forepaw holding the food pellet reached the height of the mouth. Behavioral discrete annotations were done using the JAABA program.¹⁹ For additional details, see supplemental data.

Imaging Presentation, and Data Analysis

See supplemental data.

Results

The Effect of 6-OHDA-Induced Experimental PD on Performance of the Reach-to-Grasp Motor Task

To investigate the effect of 6-OHDA-induced experimental PD on M1, we recorded from GCaMP6s-expressing M1 neurons while mice were performing a head-fixed reach-to-grasp motor task. Mice were trained to reach for food pellets located on a rotating table in front of them using their right forepaw and to bring the pellet to their mouth in response to an auditory cue (Fig. 1A, Video S1). We chose this task, as it depended on M1^{18,20} and as PD was shown to affect hand dexterity and fine motor movements.²¹

We initially performed recordings after mice reached expert levels in control conditions (>50% success rate). Later, we induced experimental PD and repeated the experiments after a minimum delay of 3 weeks (Fig. 1B). To confirm success of the PD model, we monitored spontaneous rotations in the open-field test that showed a clear ipsilateral bias²² (Fig. 1C). At the end of experiments, we histologically confirmed loss of TH immunoreactivity (Fig. 1D–F). To quantify motor performance of the reach-to-grasp task, we relied on the success rate of trials and the execution of 3 discrete motor milestone events: lift, grab, and at mouth (Fig. 1G).

The 6-OHDA-induced experimental PD markedly affected performance of the reach-to-grasp task. While under control conditions, mice attempted to grasp the food pellet in almost all trials, after 6-OHDA, during the majority of trials (65% \pm 5%) mice did not initiate movement at all (freeze trials); see Figure 1H and Video S2). In addition, parkinsonian mice were significantly less likely to successfully complete the task and consume the food pellet (Fig. 1I).

We next examined the effect of experimental PD on the task execution time. We divided the task into 3 separate time segments. First was between the auditory “go” cue (tone) and onset of a lift (initiation time). Second was between lifting the forepaw from the perch and grabbing the food pellet. And third was between grabbing the food pellet and bringing it to the mouth. We

found experimental PD increased the initiation time by almost 3-fold ($312\% \pm 2\%$), and to a lesser degree, but still significantly, prolonged the third time segment between grabbing the food pellet and bringing it to the mouth ($17\% \pm 6\%$); see Figure 1J–M and Video S3). Interestingly, striatal lesion did not significantly affect the second ballistic movement time segment between

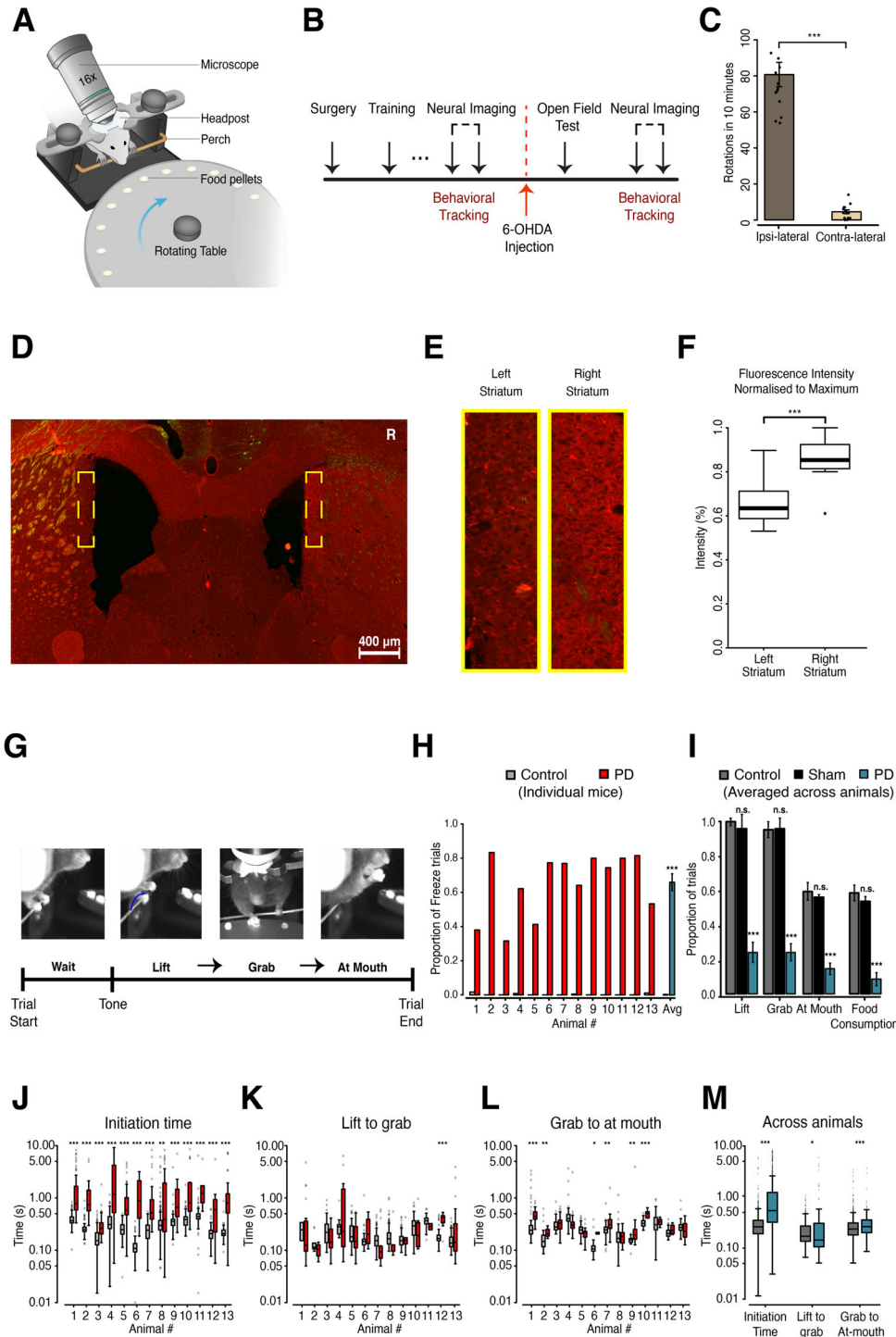


FIG. 1. Legend on next page.

lifting the forepaw and grabbing the pellet (Fig. 1K,M), indicating experimental PD did not cause general slowing of movements, but rather selectively affected movement initiation.

Effect of 6-OHDA-Induced Experimental PD on the Activity of Layer 5 PT Neurons and Layer 2/3 Pyramidal Neurons During the Reach-to-Grasp Motor Task

Concomitantly with the behavioral observations, we performed 2-photon calcium imaging to monitor the activity of 2 neuronal subpopulations in M1, the output layer 5 PT neurons and layer 2/3 PNs (Figs. 1A and 2A–G). Our experiments allowed simultaneous monitoring of multiple neurons in the same field of view (average of 180 ± 50 neurons) at single-cell resolution. We were able to repeatedly record the same neurons over multiple days and weeks relying on anatomical features of neurons and blood vessels.

To target layer 5 PT neurons, we injected retrograde viral vector (rAAV2-retro) carrying the *GCaMP6s* gene to the pons.^{2,3} Under control conditions, the vast majority of layer 5 PT neurons vigorously responded during execution of the dexterous reach-to-grasp motor task (Fig. 2A). After 6-OHDA injection, we observed marked reduction in activation intensity of PT neurons during task performance, which was more pronounced during freeze versus nonfreeze trials (Fig. 2B–D). On average experimental PD decreased peak activation of PT neurons during the task by $31\% \pm 3\%$ and $58\% \pm 4\%$, respectively, during nonfreeze and freeze trials (Fig. 2D). Application of the dopamine agonist, apomorphine significantly increased the activation intensity of layer 5 PT neurons during the reach-to-grasp motor task (Fig. 2E). However, it did not improve task outcome, possibly because of agitation and restlessness induced by apomorphine.

We next recorded the activity of layer 2/3 PNs (Fig. 2F,G). Under control conditions, at the onset of the reach-to-grasp task, layer 2/3 PNs typically exhibited a short-lived increase in activity, followed by prolonged suppression, which outlasted forelimb movements of the motor task¹⁸ (Fig. 2F,G). The initial activation phase of layer 2/3 PNs was not significantly affected by experimental PD. In contrast, the late inhibitory phase was markedly attenuated during both freeze and nonfreeze trials (Fig. 2G). These findings indicated experimental PD differentially altered the activity of different neuronal subpopulations during different phases of the response.

Direct Optogenetic Activation of M1 Pyramidal Neurons

We next examined whether direct activation of M1 PNs can improve performance of the reach-to-grasp task in experimental PD mice. We expressed channelrhodopsin-2 in M1 PNs under the CaMKII promoter, and compared task performance in experimental PD mice with and without optogenetic stimulation (2-second optostimulation starting with the tone); see Figure 2H). Optogenetic stimulation markedly reduced freezing and increased the lift probability. The probability of 6-OHDA-injected mice initiating the task and lifting their forepaw was 4 ± 2.3 times higher when optogenetic stimulation was applied (Fig. 2J). Optogenetic activation of M1 PNs also markedly shortened the initiation time (Fig. 2K). Similar results were obtained when we optogenetically activated layer 5 PT neurons (Fig. 2L). Interestingly, optogenetic activation did not improve food consumption or promote task completion beyond lift. These findings suggest that in addition to action initiation signaling, experimental PD also disrupts other intrinsic processes in M1 that are required for execution of skilled prehensile movements.

FIG. 1 PD impairs performance of the reach-to-grasp motor task. **(A)** Schematic illustration of the experimental setup showing the head-fixed mouse, the food pellets on the rotating table, and the objective used for concurrent 2-photon calcium imaging. **(B)** Experimental time line. Surgery — craniotomy and viral injection; training — mice were trained in the reach-to-grasp task until achieving expert level (>50% success rate); neural imaging/behavioral tracking — sessions of 2-photon calcium imaging while mice performed the motor task. Two sessions were performed on separate days before and another 2 at least 3 weeks after PD induction. **(C)** Comparison between ipsi- and contralateral spontaneous rotations relative to the site of 6-OHDA injection (left striatum) during a 10-minute open-field test performed after PD induction. **(D)** Fluorescent image of a 12- μ m-thick coronal slice immunohistochemically stained for the enzyme tyrosine hydroxylase (TH). The slice was obtained from a mouse injected with 6-OHDA into the left striatum, and the rAAV2 retroviral vector containing the *GCaMP6s* gene into the left pons. The image is composed of an overlay of green and red fluorescence images that visualize *GCaMP6s* and TH expression, respectively. Note the reduction of TH staining and the *GCaMP6s*-expressing axons in the left striatum. **(E)** Magnification of 2 exemplary areas, shown as yellow boxes in **(D)**, emphasizing the effect of 6-OHDA injection. **(F)** Box plots comparing the red fluorescence intensity of the injected (left) versus the uninjected (right) striatum. The midline represents the median value. **(G)** Each trial starts with a 4-second waiting period during which the mouse holds the perch and waits for an auditory “go” cue (tone), which marks table rotation and access to a new food pellet. Three discrete motor milestones were defined during the reach-to-grasp task: lift, grab and at mouth. **(H)** Proportion of freeze trials (in which mice did not initiate any movement after the tone). Data are shown for each animal separately (control, gray bars; PD, red bars), and for the average (mean \pm SEM) of all animals (rightmost bars: control, dark gray; PD, dark blue). **(I)** Average fraction of trials (mean \pm SEM) in which mice achieved the different milestones of the task for control conditions (13 mice, dark gray), sham injections (3 mice, black) and after induction of PD (13 mice, dark blue). **(J, L)** Box plots showing the time gap in seconds between tone and lift onset (initiation time, J), last lift and first grab onset (K), and last grab and at mouth (L). The data are presented for individual mice under control conditions (gray) and after induction of experimental PD (red). **(M)** Box plots showing time in seconds between the different milestones presented in **(G)** for all animals combined in control (dark gray) and PD (dark blue). Midlines represent the median. (13 mice; each mouse had 116 ± 30 control trials, and 105 ± 45 PD trials [mean \pm SD]). For all panels, Wilcoxon test * $P < 0.05$, ** $P < 0.01$, *** $P < 0.001$, n.s., statistically insignificant. [Color figure can be viewed at wileyonlinelibrary.com]

Experimental PD Disrupts Dynamics of the Layer 5 PT Network During the Reach-to-Grasp Motor Task

The M1 network serves as a dynamical system, driven internally and externally, to generate temporal sequences of output commands in a population of layer 5 PT neurons.^{10,23-25}

To capture the dynamics of the layer 5 PT neuronal population, we performed principal components analysis (PCA) on the activity of all recorded layer 5 PT neurons during the reach-to-grasp task and plotted the dynamics of the first 3 components in a 3-dimensional (3-D) space.^{11,18} Figure 3A shows examples of the time-varying trajectories from layer 5 PT network of

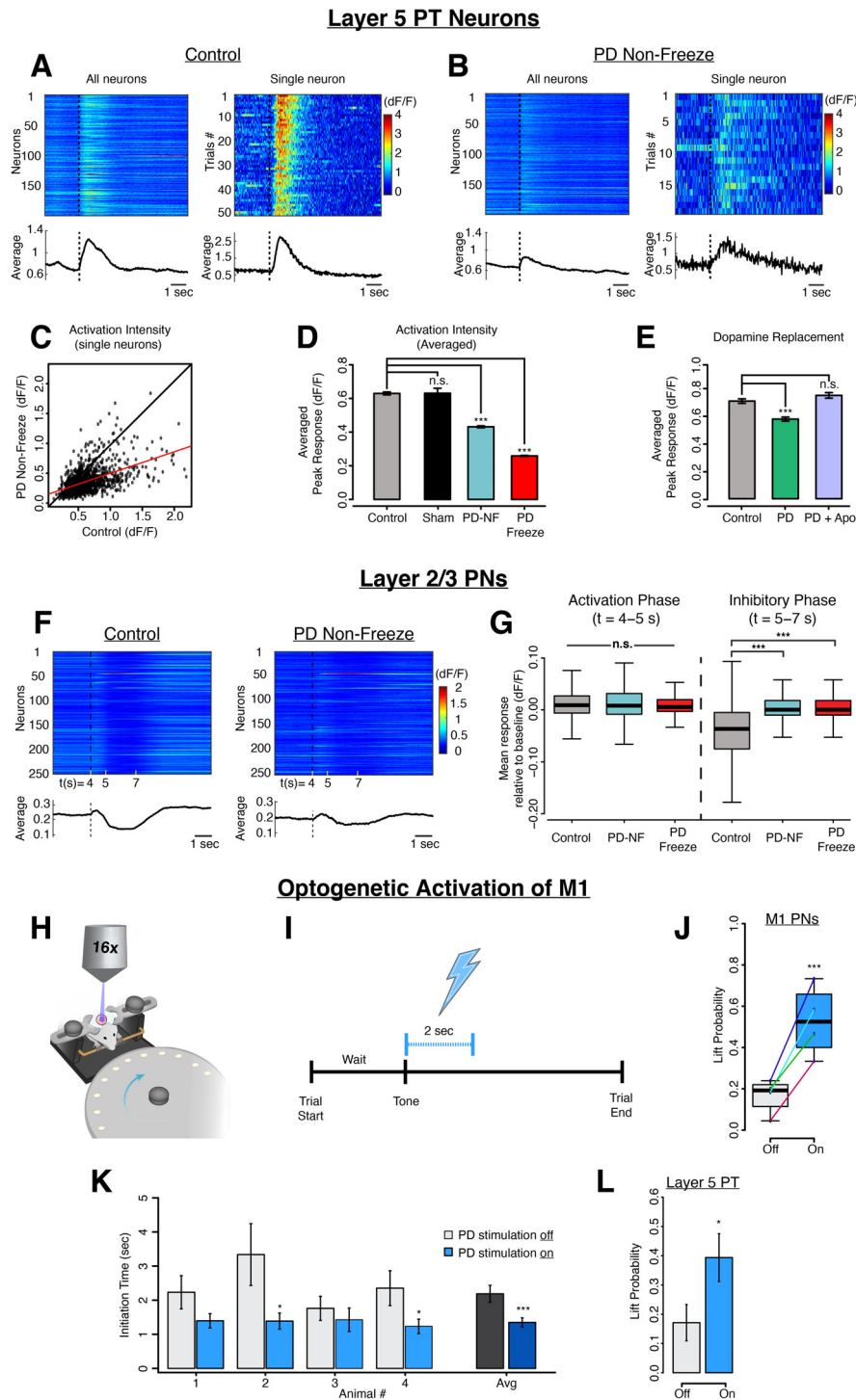


FIG. 2. Legend on next page.

2 different mice during the control period and after striatal lesion, during nonfreeze and freeze trials (Fig. 3A,B). We used sensitivity index (d') to quantify the difference between the trajectories along different time segments of the task (Fig. 3A,B, right). Whereas the initial state of the network prior to the tone was only slightly affected by experimental PD, dynamic trajectories quickly diverged from control trajectories after the tone (Fig. 3A,C) and more so in freeze versus nonfreeze trials (Fig. 3B,C).

We next calculated the length of the plotted trajectories in the 3-D space. Although the trajectories in the initial phase prior to the tone were equal or even longer after 6-OHDA, they were significantly shorter during the movement and postmovement epochs (Fig. 3D). In mice injected with 6-OHDA during the movement and postmovement epochs, freeze trials showed shorter trajectory length than nonfreeze trials (Fig. 3D).

Next, we compared the trajectories of layer 2/3 PNs during control and experimental-PD conditions. In contrast to layer 5 PT neurons, striatal lesion had no significant effect on the trajectories of layer 2/3 PNs (Fig. 3E–G).

Experimental PD Disrupts Motor Parameter Encoding During the Reach-to-Grasp Motor Task

To quantitatively correlate movement and activity of layer 5 PT and layer 2/3 PNs, we applied a generalized linear model (GLM). For each neuron we fitted the fluorescence response (dF/F) as a function of 4 discrete behavioral events — tone, lift, grab, and at mouth — and the overall predicted fluorescence response

(Fig. 4A–C). The computed prediction was then compared with the actual response recorded from the cell during the reach-to-grasp task.

The response of PT neurons became less well predicted by the GLM analysis after striatal 6-OHDA injections (Fig. 4D–F). On average, our model succeeded in explaining $25\% \pm 0.1\%$ of the variance in activity of layer 5 PT neurons under control conditions and only $9\% \pm 0.02\%$ after induction of experimental PD (1128 neurons from 7 mice, $P < 0.001$; Fig. 4F). Similar results were acquired for layer 2/3 PNs (Fig. 4F), although the GLM of calcium transients generated by layer 2/3 PNs was much less effective in modeling discrete events of the reach-to-grasp task compared with layer 5 PT neurons.¹⁸

Our experiments enabled us to record the same neurons in numerous daily sessions over multiple days. Specifically, in each mouse daily we performed 4 recording sessions: 2 control sessions and 2 additional sessions at least 3 weeks after 6-OHDA injections. We focused on 444 layer 5 PT neurons (7 mice, 39.4% of all recorded neurons) that were imaged in all recording sessions, in which the GLM explained at least 20% of their overall activity in the first recording session. The GLM model parameters of the 2 control sessions showed the greatest similarity (65% had Pearson's correlation coefficient > 0.5 ; Fig. 4G, upper), indicating relatively high stability of motor encoding of a learned dexterous task. Coding stability between the 2 experimental PD sessions was much smaller, with only 20% of neurons showing a Pearson's correlation coefficient above 0.5 and most neurons showing a cross-session Pearson's correlation coefficient near zero (Fig. 4G,

FIG. 2 Experimental PD differentially affects activation of layer 5 PT neurons and layer 2/3 PNs in M1 and optogenetic activation of M1 pyramidal neurons reversed PD motor initiation impairment. **(A, B)** Examples of 2-photon traces for averaged activity of all neurons sharing the same field of view (FOV) in a single experimental session (left) as well as single neuron activity in different trials within a session (right) in control and PD nonfreeze trials. X axis represents time (seconds), and Y axis represents the different recorded PT neurons in the left panels and the different trials for the same exemplary neuron in the right panels. The fluorescence intensity (dF/F) is presented by a color map. In the left, for each neuron each line represents the averaged activity in all trials of the session. The black trace represents the averaged activity of all neurons combined and the dashed black vertical line represents the time of tone. **(C)** For each individual neuron we compared the peak value of the trial-averaged response (dF/F) recorded during control (X-axis value) and PD nonfreeze (Y-axis value) trials. Data are shown for all recorded individual neurons from all animals (7 mice, 1128 neurons). Black line shows equality between normal and PD conditions, and red line shows the best linear fit of all points. **(D)** Averaged peak dF/F responses (mean \pm SEM) were compared between 4 different conditions: control, sham lesion; PD nonfreeze and PD Freeze trials (7 mice, 1128 neurons for control and PD; 3 mice, 500 neurons for sham). **(E)** Averaged peak dF/F responses (mean \pm SEM) are presented for 3 conditions: control, PD and PD after subcutaneous application of the dopamine receptor agonist apomorphine hydrochloride (PD + Apo, 2 mice, 310 neurons). **(F)** Averaged 2-photon activity traces of all neurons sharing the same FOV in a single mouse obtained from a single control session (left) and nonfreeze trials from a single PD session (right). X axis represents time, and Y axis represents the different recorded layer 2/3 PNs. Each line represents the average activity of a neuron in all trials of the session. The fluorescence intensity (dF/F) is presented by a color map. The black trace underneath represents the averaged activity of all neurons. The dashed black vertical line represents the time of tone. **(G)** Box plots showing the averaged peak values relative to baseline of the initial activation phase (0–1 seconds after the tone) and sequential inhibition phase (1–3 seconds after the tone) obtained from all recorded neurons. Midlines represent the median (4 mice, 762 neurons). **(H)** Schematic diagram of the optogenetic experimental setup. A craniotomy with a glass coverslip was constructed over M1. Channelrhodopsin was activated by 470-nm laser pulse trains. In addition, a blue LED pointing to the mouse face was activated continuously to mask any visual effect of the optogenetic activation. **(I)** Experimental time line of the optogenetic stimulation sessions. A 2-second optogenetic stimulation was administered, starting at the tone. **(J)** Comparison of the averaged lift probability with (blue) and without (light gray) optogenetic stimulation of M1 PNs. The colored lines connect the average values for each individual mouse (4 mice). Lift probability was calculated as the proportion of trials in which mice lifted their forepaw within 2 seconds following the tone. **(K)** The averaged (mean \pm SEM) initiation time (time between tone and lift) in nonfreeze trials is plotted under control conditions (light gray) and during optogenetic stimulation (blue). Data are shown for each individual mouse (left, light gray and light blue) and for the averaged results of all trials in all mice (right, dark gray and dark blue). X axis specifies the animal, and Y axis shows time in seconds. Seventy-two unstimulated trials and 133 stimulated trials in 4 mice. **(L)** Same as **(J)** for layer 5 PT neuron-specific optogenetic activation. See Methods section (2 mice, 50 unstimulated trials and 60 stimulated). * $P < 0.05$, *** $P < 0.001$ using the Wilcoxon test. [Color figure can be viewed at wileyonlinelibrary.com]

middle). Comparing the last control session with the first experimental PD session showed even lower correlation between their modeled parameters (Fig. 4G, lower). Thus, experimental PD not only weakened motor encoding of motor parameters during the learned reach-to-grasp task within a session, but also diminished intersession stability of motor parameters encoding the M1 layer 5 PT network.

Experimental PD Disrupts Intratrial Recruitment Synchrony and Intertrial Activation Reproducibility of Layer 5 PT Neurons During the Reach-to-Grasp Motor Task

We next investigated the effect of experimental PD on synchrony of PT neurons within the same trial and their activation reproducibility during repeated trials

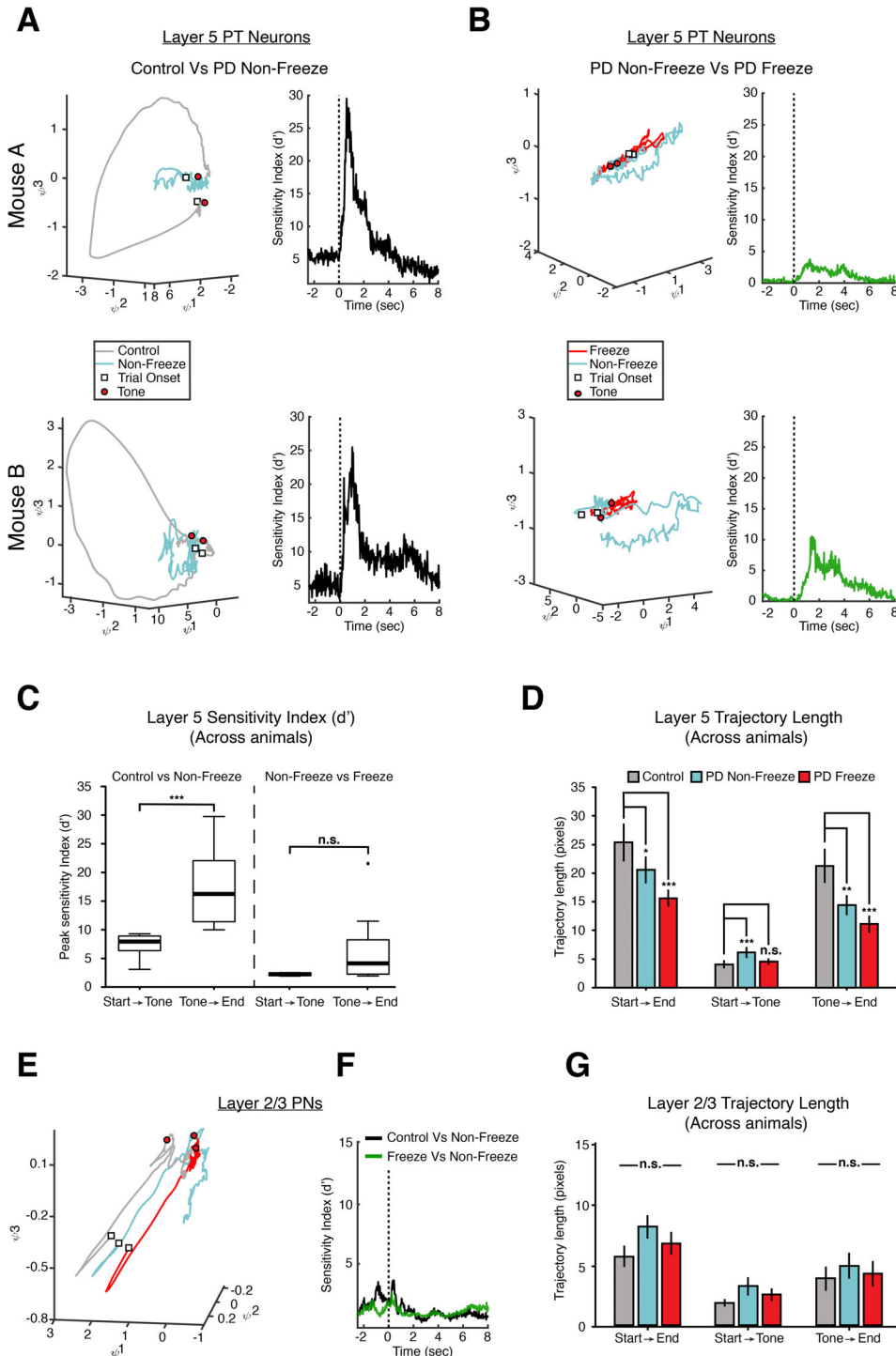


FIG. 3. Legend on next page.

within the same session. To investigate synchronization of the different recorded neurons during a trial, we compared the averaged pairwise Pearson's correlation coefficient between PT neurons before and after 6-OHDA injection. We found experimental PD significantly reduced recruitment synchronization of PT neurons during individual trials (Fig. 5A). During the reach-to-grasp task, the averaged Pearson's correlation coefficient between pairs of PT neurons during individual trials decreased from 0.27 ± 0.005 under control conditions to 0.16 ± 0.004 in experimental PD ($P < 0.001$).

To characterize the intertrial activation reproducibility within the same daily session, for each neuron we calculated the pairwise Pearson's correlation coefficient between the activity traces of all possible trial pair combinations obtained during the session. Next, we calculated the averaged coefficient for each neuron and for all recorded neurons for the entire session. We found the average intertrial Pearson's correlation coefficient was significantly reduced during nonfreeze experimental PD trials compared with control conditions and further dramatically dropped during freeze trials (Fig. 5B).

Experimental PD Disrupts Intersession Temporal Recruitment Stability of Layer 5 PT Neurons During the Reach-to-Grasp Motor Task

We next investigated the stability of the temporal recruitment of layer 5 PT neurons during repeated sessions recorded over multiple days. In these experiments, we measured the time to peak of the averaged responses for each neuron and ranked the neurons relative to others in the same field of view based on this measure. For this analysis we only included neurons that were recorded in all 4 consecutive sessions: 2 control sessions and 2 postlesion sessions (1128 neurons from 7 mice). Figure 5C,D presents the responses in 3 consecutive sessions: 2 control sessions and 1 experimental PD session. The trials of the experimental PD session were divided into freeze and nonfreeze trials, and neurons in all

3 sessions were ranked according to the time of activation peak in the first control session. The findings reveal temporal recruitment was relatively conserved between the 2 control days (Fig. 5C). Conversely, a strong loss of the temporal recruitment order was observed in the nonfreeze trials, and a total disarrangement of the temporal recruitment in the freeze trials was evident (Fig. 5D).

To quantify stability of the temporal recruitment across days, we used 2 metrics. First, we measured the averaged absolute time in which each neuron reached its maximal intensity in a single experimental session. Second, we enumerated the neurons for each day according to their temporal recruitment order. The results show that although the temporal recruitment was relatively preserved between control sessions, it was markedly disrupted when comparing control and experimental PD sessions as well as comparing 2 consecutive sessions after 6-OHDA injections (Fig. 5E–H). The averaged Spearman's correlation coefficients between the ranking order of 2 daily sessions decreased from 0.53 ± 0.05 when comparing 2 control sessions with 0.17 ± 0.04 for comparison between nonfreeze trials of 2 PD sessions ($P < 0.01$). Taken together, our findings show experimental PD disrupts neuron-to-neuron synchrony, intertrial activation reproducibility, and cross-day stability of the temporal recruitment of the layer 5 PT population during performance of the skilled prehensile motor task.

Discussion

The main findings of our study are: (1) 6-OHDA-induced experimental PD markedly impaired performance of the reach-to-grasp motor task and especially disrupted initiation of the task. Optogenetic activation of M1 during task performance partially rescued movement initiation. (2) At the single-cell level, experimental PD affected M1 in a cell-type-specific manner. Although markedly suppressing activation of layer 5 PT neurons, movement-related activation of layer 2/3

FIG. 3 PD disrupts population network dynamics of layer 5 PT neurons during reach-to-grasp task. **(A)** Neural population dynamics of layer 5 PT neurons in 2 different mice in which control trials were compared with nonfreeze trials. Left panels depict the main 3 components obtained by using PCA plotted in a 3-D space. The white square marks trial onset, and red circle marks the time of tone (4 seconds). Right panels present the sensitivity index (d') plotted over time for comparison of the 2 trajectories presented in the left panels. Dashed line marks the tone. **(B)** Same as **(A)** for comparison of freeze and nonfreeze trials within PD sessions. **(C)** Summary of the peak sensitivity index (d') measurements comparing control versus nonfreeze PD trials (left) and freeze versus nonfreeze PD trials (right) during 2 different time segments of the trial, the premovement initial state (start to tone) and after the tone (tone to trial end, 4–12 seconds). **(D)** Average (median \pm SEM) trajectory length is calculated for 3 different time windows for control, PD nonfreeze and PD freeze trials. The time windows for each condition include start to end (0–12 seconds), start to tone (0–4 seconds), and tone to end (4–12 seconds). For the analysis presented in **(C)** and **(D)**, 580 control trials and 556 PD trials from 7 mice were used. **(E)** Neural population dynamics of layer 2/3 PNs in a single mouse are shown for all trials of a control session (gray), Nonfreeze (light blue) and freeze PD (red) trials from a single session. The graph depicts the main 3 components obtained by using PCA plotted in a 3-D space. The white square marks the trial's onset, and the red circle marks the time of tone (4 seconds). **(F)** Sensitivity index (d') plotted over time for comparison of the different trajectories presented in **(E)**. Black trace for comparison of control and PD nonfreeze trials. Green trace for comparison of freeze and nonfreeze PD trials. Dashed line marks the tone. **(G)** Average (median \pm SEM) trajectory length is calculated for 3 different time windows for control, PD nonfreeze, and PD freeze trials as explained in **(D)**. For the analysis presented, 367 control trials and 260 PD trials from 4 mice were used. * $P < 0.05$, ** $P < 0.01$, *** $P < 0.001$. n.s., statistically insignificant. [Color figure can be viewed at wileyonlinelibrary.com]

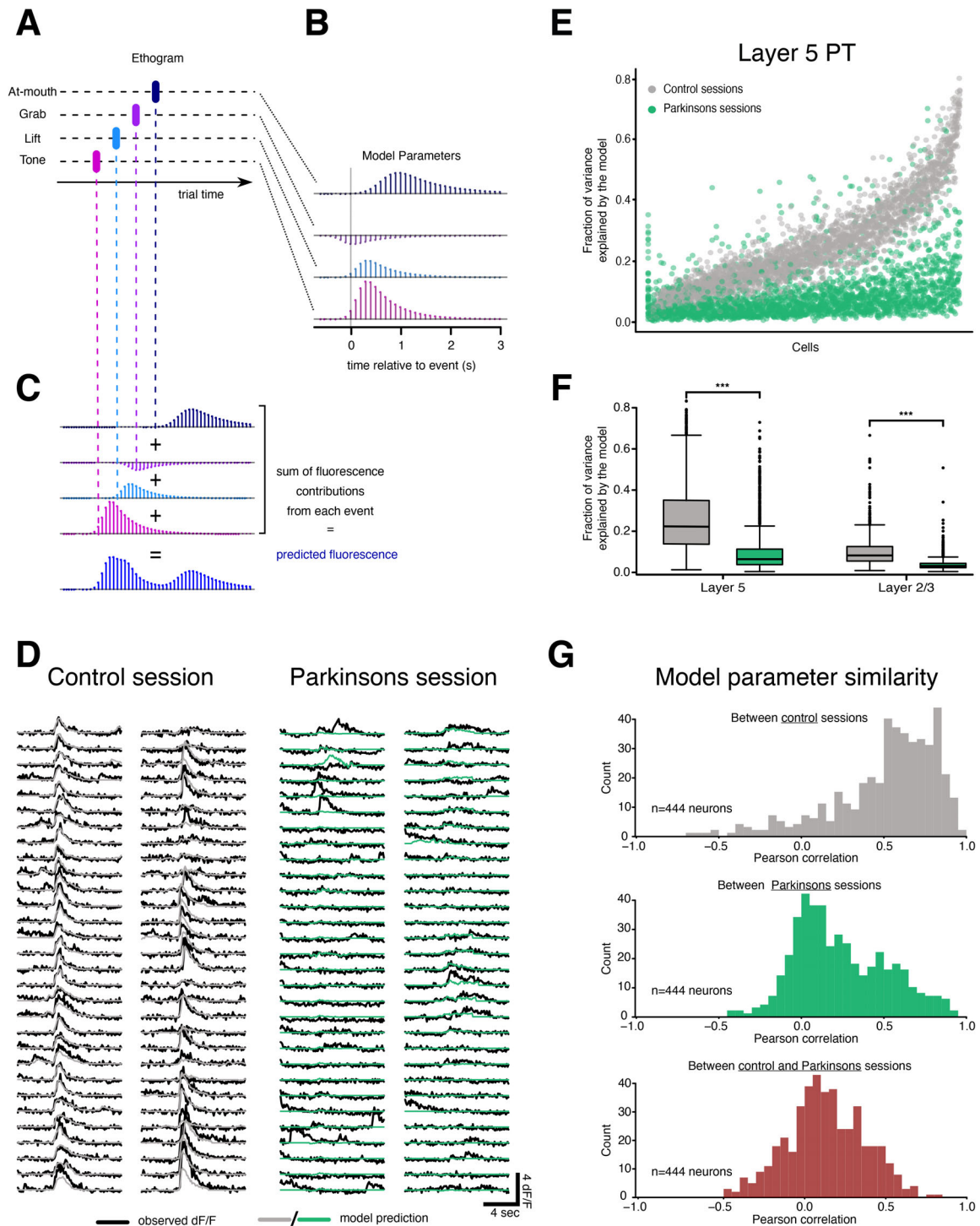


FIG. 4. PD impairs layer 5 PT neuron motor parameters encoding and stability. **(A)** Illustrative synthetic example ethogram containing 4 sequential events in a single trial. **(B)** Example synthetic model parameters for a single neuron indicating its fluorescence responses to the 4 behavioral events shown in **(A)**. **(C)** Fluorescence prediction for the synthetic neuron shown in **(B)** under a linear model. For each neuron, the predicted fluorescence is a linear combination of the ethogram convolved with the model parameters. **(D)** Examples of actual and modeled fluorescence traces during single sessions for 2 different neurons in 1 control session (left 2 columns) and 1 PD session (right 2 columns). Each row shows the measured fluorescence (dF/F) for a single 12-second trial (black) and the prediction from the linear model for control (gray) or PD (green) sessions based on behavioral events that occurred during that trial. **(E)** Mean predictability for all individual layer 5 PT neurons during control (gray) and PD (green) sessions for all mice. Mean predictability was quantified as the fraction of variance explained by the model, where 1 is a perfect prediction and 0 means no better than simply predicting a constant fluorescence value (7 mice, 1128 neurons for layer 5 PTs). Neurons were sorted along the X axis by their mean predictability on control days. **(F)** Box plots showing GLM model predictability in layer 5 PT neurons (left) and layer 2/3 PNs (right, 762 neurons in 4 mice) during control and PD sessions. Midlines represent the median. **(G)** Model parameter similarity between control sessions (upper panel), 2 consecutive PD sessions (middle panel), and the last control and first PD session (lower panel) calculated as Pearson's correlation coefficient between vectors of model parameters. This analysis was done on 444 layer 5 PT neurons, for which the model could explain greater than 20% of the variance in fluorescence. *** $P < 0.001$. [Color figure can be viewed at wileyonlinelibrary.com]

PNs was not significantly affected. (3) At the neuronal population level, experimental PD markedly disrupted layer 5 PT population dynamics while only minimally affecting that of layer 2/3 PNs. (4) Experimental PD impaired activation accuracy of layer 5 PT neurons, shown by disruption of the intratrial synchronization of the different PT neurons, as well as their intertrial

activation reproducibility during task performance. (5) Finally, experimental PD markedly impaired the cross-day stability of the PT network both with respect to motor parameter encoding and the temporal recruitment.

Our study was mostly descriptive, and aside from the optogenetics, we did not directly address the mechanisms

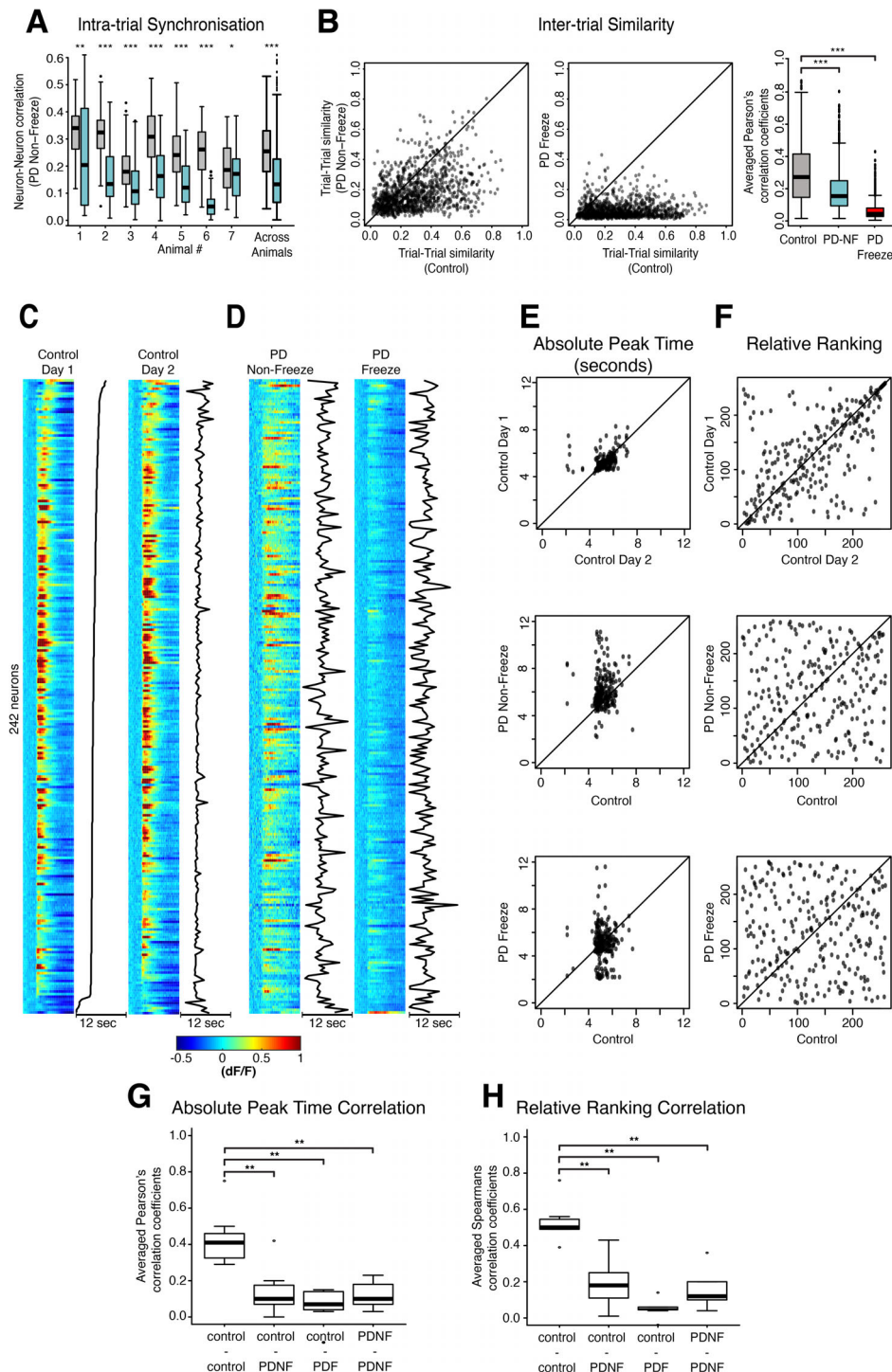


FIG. 5. Legend on next page.

underlying the effect of experimental PD on the M1 cortex. However, our findings allow us to speculate that impaired motor performance in experimental PD resulted from disruption of 2 mechanisms. Impaired external thalamocortical action initiation driving, and disruption of the intrinsic M1 connectivity and dynamics.

In our study we used the 6-OHDA hemi-PD model, which mimics a key feature of PD, dopamine depletion in the striatum. Yet it differs from human PD disease in several features, including neurodegeneration of other, nondopaminergic neurons; acute versus insidious onset of dopamine depletion; and unilateral versus bilateral, albeit asymmetrical, dopamine depletion in human disease.

A leading theory regarding the pathogenesis of PD attributes motor disability to reduced driving of the M1 network by the cortical-BG loop.^{26,27} Interestingly, both the classical rate model⁴ and center-surround model^{28,29} anticipate reduced firing of M1 neurons in PD.³⁰ Consistent with this prediction, we observed reduction in movement-related firing of layer 5 PT neurons, which may have resulted from loss of direct thalamocortical (TC) input activation of M1 PT neurons.³¹⁻³³ These results are consistent with findings of previous studies in 1-methyl-4-phenyl-1,2,3,6-tetrahydropyridine (MPTP)-treated primates,^{16,34} which also demonstrated reduced activation and attenuated motor parameter encoding of PT neurons. However, in contrast to previous primate studies, we observed cell-type-specific effects of experimental PD. Although activation of layer 5 PT was attenuated, experimental PD did not significantly affect the initial activation phase of layer 2/3 PNs. Rather, it decreased the amplitude of the second inhibitory phase that normally followed and outlasted forelimb movement. These findings indicate that the hypothesis claiming global suppression of M1 in PD is oversimplified. The mechanisms underlying the differential effects of experimental PD on different cell populations in M1 are still unclear. It may be related to differential innervation of layer 5 PT and layer 2/3 neurons by TC

inputs.^{32,33} Alternatively, it may result from reduced feed-forward inhibition of layer 2/3 PNs. A second difference between our findings and prior primate studies is related to synchronization of M1 neurons. Although synchronization was reported to increase in MPTP-treated monkeys,^{35,36} we showed decreased synchronization of PT neurons during the reach-to-grasp task. These differences may be related to differences in animal models, recording techniques, and, most importantly, that our recordings were obtained during voluntary motor task performance, whereas the primate studies examined synchrony during rest or passive limb manipulation.

Striatal dopamine deficiency is expected to increase activity of the indirect pathway.^{3,4} Thus, our findings are consistent with a previous study showing suppressed firing of most M1 neurons in response to optogenetic activation of the striatal medium spiny neurons belonging to the indirect pathway.³⁷

Previous studies have shown the importance of the cortico-BG loop in action initiation and selection of motor tasks.³⁸⁻⁴⁰ Consistent with these reports, we demonstrated that experimental PD markedly disrupted initiation of the reach-to-grasp task. The attenuated movement-related activation of layer 5 PT neurons in the parkinsonian M1 probably contributed to impaired action initiation in experimental PD. Yet our combined results indicated that in addition to disrupting task initiation, experimental PD also intrinsically affected the M1 network.

Consistent with the involvement of M1 in the pathogenesis of PD, previous studies have described various abnormalities in the M1 of parkinsonian patients and PD models, including increased beta activity of local field potentials and electroencephalogram,^{14,30,41-47} attenuated motor parameter encoding and increased pairwise synchronization of M1 neurons in MPTP-treated monkeys,^{16,35,36,48-51} as well as functional imaging abnormalities in the M1 of PD patients.⁵²

At the population level M1 can be regarded as a dynamic system generating temporally precise

FIG. 5 PD disrupts intra-trial activation synchrony, intertrial activation reproducibility, and cross-day temporal recruitment stability of layer 5 PT neurons during the reach-to-grasp task. **(A)** Averaged pairwise Pearson's correlation coefficient between the activity of recorded layer 5 PT neurons within each trial is calculated for control (gray) and PD nonfreeze conditions (time window is -1 to $+2$ seconds relative to tone). The synchrony comparisons within single animals and across all animals are presented. For each trial, the Pearson's correlation coefficient was calculated for all possible neuronal pair combinations and averaged over the entire individual trials. Next, an average value for all trials within a daily session is obtained. **(B)** Averaged temporal Pearson's correlation coefficient between all possible pairs of trials for each single layer 5 PT neuron (same time window as in [A]). The comparison is made between activity traces in control (X axis) and PD nonfreeze trials (left panel) or freeze trials (middle panel). The rightmost panel summarizes the results using box plots for all animals combined. **(C, D)** Exemplary layer 5 PT neuronal averaged activity from a single mouse sorted by the time of peak response in the first control session (left panel in [C]). After the neuronal order was determined, it was then copied to the following 3 color maps showing the activity of the same set of neurons (242 neurons) in control and PD conditions. The averaged activity of all trials in the session is shown in a color map. The black lines connect the different neurons' peak activity points. **(C)** Two consecutive control sessions. **(D)** Nonfreeze and freeze trials in 1 PD session. **(E, F)** For each PT neuron presented in **(D)**, the averaged absolute activity peak time in seconds **(E)** and the averaged relative rank among other neurons within the field of view **(F)** is calculated. Then, a comparison of the 2 metrics is made between the 2 control sessions, control and nonfreeze trials and finally between control and freeze trials. **(G, H)** Box plots summarizing the results of the 2 metrics shown in **(E, F)** for the different possible session-type combinations. Midlines represent the median (7 mice, 1128 layer 5 PT neurons; * $P < 0.05$, ** $P < 0.01$, *** $P < 0.001$). [Color figure can be viewed at wileyonlinelibrary.com]

sequences of output motor commands in layer 5 PT neurons to control dexterous movements.^{10,11,13,24,53} Performance of learned dexterous motor tasks in this dynamic system depends on the initial state of M1 network, external inputs to M1, and the internal dynamics of the M1 network.^{25,53} Our data indicate experimental PD disrupts both external driving and internal dynamics of M1. Disruption of action initiation resulted from attenuated external driving of M1 by TC inputs carrying BG information, but what is the source of impairment of internal population dynamics of the PT subnetwork in experimental PD? M1 has been strongly implicated in motor learning, especially of dexterous movements.⁵⁴ It undergoes structural plasticity changes as well as network changes such as temporal sharpening and increased synchronized activation of subgroups of neurons.⁵⁵⁻⁵⁹ We speculate that the M1 network in PD may undergo a “delearning” process, caused by loss of connectivity generated during learning, and expressing as impaired internal dynamics, diminished activation temporal accuracy, and loss of stability of the PT subnetwork. Consistent with this possibility are the increased turnover of dendritic spines in the parkinsonian M1¹⁵ and our findings regarding loss of stability of temporal recruitment and motor encoding of layer 5 PT neurons after induction of experimental PD.⁵⁶

A recent provocative article⁶⁰ hypothesized that M1 contributes to the neurodegenerative process of PD via the activity of corticostriatal inputs. This hypothesis is primarily based on somatotopical manifestations of PD symptoms that cannot be attributed to the neurodegenerative process of the dopaminergic neurons in the substantia nigra, which has no known somatotopic representation. Here we propose an alternative explanation for the somatotopic symptomatology, secondary changes induced by PD to M1.

Further studies are required to dissect the mechanisms responsible for the changes induced by PD to the M1 PT network and to establish new treatment strategies, possibly by novel cortical or thalamic neurostimulation paradigms, to counterbalance these changes and improve motor disability in PD patients. ■

References

- Poewe W, Seppi K, Tanner CM, et al. Parkinson disease. *Nat Rev Dis Prim* 2017;3(1):1-21.
- Armstrong MJ, Okun MS. Diagnosis and treatment of Parkinson disease: a review. *J Am Med Assoc* 2020;323(6):548-560.
- Calabresi P, Picconi B, Tozzi A, Ghiglieri V, Di Filippo M. Direct and indirect pathways of basal ganglia: a critical reappraisal. *Nat Neurosci* 2014;17(8):1022-1030.
- Nelson AB, Kreitzer AC. Reassessing models of basal ganglia function and dysfunction. *Annu Rev Neurosci* 2014;37(1):117-135.
- Simonyan K. Recent advances in understanding the role of the basal ganglia. *F1000Res* 2019;8:122.
- Hintiryan H, Foster NN, Bowman I, et al. The mouse cortico-striatal projectome. *Nat Neurosci* 2016;19(8):1100-1114.
- Anderson CT, Sheets PL, Kiritani T, Shepherd GMG. Sublayer-specific microcircuits of corticospinal and corticostriatal neurons in motor cortex. *Nat Neurosci* 2010;13(6):739-744.
- Lemon RN, Johansson RS, Westling G. Corticospinal control during reach, grasp, and precision lift in man. *J Neurosci* 1995;15(9):6145-6156.
- Shepherd GMG. Corticostriatal connectivity and its role in disease. *Nat Rev Neurosci* 2013;14(4):278-291.
- Isomura Y, Harukuni R, Takekawa T, Aizawa H, Fukai T. Microcircuitry coordination of cortical motor information in self-initiation of voluntary movements. *Nat Neurosci* 2009;12(12):1586-1593.
- Shenoy KV, Sahani M, Churchland MM. Cortical control of arm movements: a dynamical systems perspective. *Annu Rev Neurosci* 2013;36(1):337-359.
- Churchland MM, Cunningham JP. A dynamical basis set for generating reaches. *Cold Spring Harb Symp Quant Biol* 2014;79:67-80.
- Kaufman MT, Seely JS, Sussillo D, Ryu SI, Shenoy KV, Churchland MM. The largest response component in the motor cortex reflects movement timing but not movement type. *eNeuro* 2016;3(4):ENEURO.0085-16.2016.
- Arbuthnott GW, Garcia-Munoz M. Are the symptoms of parkinsonism cortical in origin? *Comput Struct Biotechnol J* 2017;15:21-25.
- Guo L, Xiong H, Kim J-I, et al. Dynamic rewiring of neural circuits in the motor cortex in mouse models of Parkinson's disease. *Nat Neurosci* 2015;18(9):1299-1309.
- Pasquereau B, DeLong MR, Turner RS. Primary motor cortex of the parkinsonian monkey: altered encoding of active movement. *Brain* 2016;139(1):127-143.
- Aeed F, Shnitzer T, Talmon R, Schiller Y. Layer- and cell-specific recruitment dynamics during epileptic seizures in vivo. *Ann Neurol* 2020;87(1):97-115.
- Levy S, Lavzin M, Benisty H, et al. Cell-type-specific outcome representation in the primary motor cortex. *Neuron* 2020;107(5):954-971.e9.
- Kabra M, Robie AA, Rivera-Alba M, Branson S, Branson K. JAABA: interactive machine learning for automatic annotation of animal behavior. *Nat Methods* 2013;10(1):64-67.
- Guo J-Z, Graves AR, Guo WW, et al. Cortex commands the performance of skilled movement. *Elife* 2015;4(2015):1-18.
- Nakamura K, Christine CW, Starr PA, Marks WJ. Effects of unilateral subthalamic and pallidal deep brain stimulation on fine motor functions in Parkinson's disease. *Mov Disord* 2007;22(5):619-626.
- Cenci MA, Lundblad M. Ratings of L-DOPA-induced dyskinesia in the unilateral 6-OHDA lesion model of Parkinson's disease in rats and mice. *Curr Protoc Neurosci* 2007;41(1):9.25.1-9.25.23.
- Whishaw IQ, Gorny B, Sarna J. Paw and limb use in skilled and spontaneous reaching after pyramidal tract, red nucleus and combined lesions in the rat: behavioral and anatomical dissociations. *Behav Brain Res* 1998;93(1-2):167-183.
- Wang X, Liu Y, Li X, et al. Deconstruction of Corticospinal circuits for goal-directed motor skills. *Cell* 2017;171(2):440-455.e14.
- Sauerbrei BA, Guo J-Z, Cohen JD, et al. Cortical pattern generation during dexterous movement is input-driven. *Nature* 2020;577(7790):386-391.
- DeLong MR, Wichmann T. Basal ganglia circuits as targets for neuromodulation in Parkinson disease. *JAMA Neurol* 2015;72(11):1354-1360.
- Przedborski S. The two-century journey of Parkinson disease research. *Nat Rev Neurosci* 2017;18(4):251-259.
- Mink JW. The basal ganglia: focused selection and inhibition of competing motor programs. *Prog Neurobiol* 1996;50(4):381-425.
- Nambu A, Tachibana Y, Chiken S. Cause of parkinsonian symptoms: firing rate, firing pattern or dynamic activity changes? *Basal Ganglia* 2015;5(1):1-6.
- McGregor MM, Nelson AB. Circuit mechanisms of Parkinson's disease. *Neuron* 2019;101(6):1042-1056.
- Hooks BM, Mao T, Gutnisky DA, Yamawaki N, Svoboda K, Shepherd GMG. Organization of cortical and thalamic input to

- pyramidal neurons in mouse motor cortex. *J Neurosci* 2013;33(2):748–760.
32. Kaneko T. Local connection of excitatory neurons in rat motor-associated cortical areas. *Front Neural Circuits* 2013;7:75.
 33. Kuramoto E, Furuta T, Nakamura KC, Unzai T, Hioki H, Kaneko T. Two types of thalamocortical projections from the motor thalamic nuclei of the rat: a single neuron-tracing study using viral vectors. *Cereb Cortex* 2009;19(9):2065–2077.
 34. Pasquereau B, Turner RS. Primary motor cortex of the Parkinsonian monkey: differential effects on the spontaneous activity of pyramidal tract-type neurons. *Cereb Cortex* 2011;21(6):1362–1378.
 35. Goldberg JA, Boraud T, Maraton S, Haber SN, Vaadia E, Bergman H. Enhanced synchrony among primary motor cortex neurons in the 1-Methyl-4-Phenyl-1,2,3,6-Tetrahydropyridine primate model of Parkinson's disease. *J Neurosci* 2002;22(11):4639–4653.
 36. McCairn KW, Turner RS. Pallidal stimulation suppresses pathological dysrhythmia in the parkinsonian motor cortex. *J Neurophysiol* 2015;113(7):2537–2548.
 37. Oldenburg IA, Sabatini BL. Antagonistic but not symmetric regulation of primary motor cortex by basal ganglia direct and indirect pathways. *Neuron* 2015;86(5):1174–1181.
 38. Cox J, Witten IB. Striatal circuits for reward learning and decision-making. *Nat Rev Neurosci* 2019;20(8):482–494.
 39. Garr E. Contributions of the basal ganglia to action sequence learning and performance. *Neurosci Biobehav Rev* 2019;107:279–295.
 40. Klaus A, Alves da Silva J, Costa RM. What, if, and when to move: basal ganglia circuits and self-paced action initiation. *Annu Rev Neurosci* 2019;42(1):459–483.
 41. Brittain JS, Brown P. Oscillations and the basal ganglia: motor control and beyond. *Neuroimage* 2014;85:637–647.
 42. Hammond C, Bergman H, Brown P. Pathological synchronization in Parkinson's disease: networks, models and treatments. *Trends Neurosci* 2007;30(7):357–364.
 43. Lindenbach D, Bishop C. Critical involvement of the motor cortex in the pathophysiology and treatment of Parkinson's disease. *Neurosci Biobehav Rev* 2013;37(10):2737–2750.
 44. Quiroga-Varela A, Walters JR, Brazhnik E, Marin C, Obeso JA. What basal ganglia changes underlie the parkinsonian state? The significance of neuronal oscillatory activity. *Neurobiol Dis* 2013;58:242–248.
 45. Singh A. Oscillatory activity in the cortico-basal ganglia-thalamic neural circuits in Parkinson's disease. *Eur J Neurosci* 2018;48(8):2869–2878.
 46. Brazhnik E, Cruz AV, Avila I, et al. State-dependent spike and local field synchronization between motor cortex and substantia nigra in hemiparkinsonian rats. *J Neurosci* 2012;32(23):7869–7880.
 47. Delaville C, Cruz AV, McCoy AJ, et al. Oscillatory activity in basal ganglia and motor cortex in an awake behaving rodent model of Parkinson's disease. *Basal Ganglia* 2014;3(4):221–227.
 48. Parr-Brownlie LC. Bradykinesia induced by dopamine D2 receptor blockade is associated with reduced motor cortex activity in the rat. *J Neurosci* 2005;25(24):5700–5709.
 49. De Hemptinne C, Swann NC, Ostrem JL, et al. Therapeutic deep brain stimulation reduces cortical phase-amplitude coupling in Parkinson's disease. *Nat Neurosci* 2015;18(5):779–786.
 50. Galvan A, Devergnas A, Wichmann T. Alterations in neuronal activity in basal ganglia-thalamocortical circuits in the parkinsonian state. *Front Neuroanat* 2015;9:1–21.
 51. Hyland BI, Seeger-Armbruster S, Smither RA, Parr-Brownlie LC. Altered recruitment of motor cortex neuronal activity during the grasping phase of skilled reaching in a chronic rat model of unilateral parkinsonism. *J Neurosci* 2019;39(48):9660–9672.
 52. Burciu RG, Vaillancourt DE. Imaging of motor cortex physiology in Parkinson's disease. *Mov Disord* 2018;33(11):1688–1699.
 53. Kaufman MT, Churchland MM, Ryu SI, Shenoy KV. Cortical activity in the null space: permitting preparation without movement. *Nat Neurosci* 2014;17(3):440–448.
 54. Xu T, Yu X, Perlik AJ, et al. Rapid formation and selective stabilization of synapses for enduring motor memories. *Nature* 2009;462(7275):915–919.
 55. Masamizu Y, Tanaka YR, Tanaka YH, et al. Two distinct layer-specific dynamics of cortical ensembles during learning of a motor task. *Nat Neurosci* 2014;17(7):987–994.
 56. Peters AJ, Chen SX, Komiyama T. Emergence of reproducible spatiotemporal activity during motor learning. *Nature* 2014;510(7504):263–267.
 57. Peters AJ, Liu H, Komiyama T. Learning in the rodent motor cortex. *Annu Rev Neurosci* 2017;40(1):77–97.
 58. Li Q, Ko H, Qian ZM, et al. Refinement of learned skilled movement representation in motor cortex deep output layer. *Nat Commun* 2017;8(1):15834.
 59. Lemke SM, Ramanathan DS, Guo L, Won SJ, Ganguly K. Emergent modular neural control drives coordinated motor actions. *Nat Neurosci* 2019;22(7):1122–1131.
 60. Foffani G, Obeso JA. A cortical pathogenic theory of Parkinson's disease. *Neuron* 2018;99(6):1116–1128.

Supporting Data

Additional Supporting Information may be found in the online version of this article at the publisher's web-site.

SGML and CITI Use Only
DO NOT PRINT

Author Roles

F.A. conducted the experiments, analysis, and writing.

N.C. conducted analysis.

J.S. and Y.Sv conceived and supervised the project and wrote the article.

Y.Sv conceived and supervised the project and wrote the article with significant input from all authors.